Electronic Supplementary Material (ESI) for Physical Chemistry Chemical Physics.
This journal is © the Owner Societies 2021

# *In-situ* Investigation of Oxidation Across a Heterogeneous Nanoparticle-Support Interface During Metal Support Interactions-Electronic Supporting Information

**Abheek Datta[a]*, Shubham Deolka[a], Pawan Kumar[a], Zakaria Ziadi[a], Toshio Sasaki[b], Stephan Steinhauer[a], Vidyadhar Singh[a,c], Nan Jian[a,d], Eric Danielson[a], Alexander James Porkovich[a]***

[a] Okinawa Institute of Science and Technology (OIST) Graduate University, 1919-1 Tancha, Onna-Son, Okinawa 904-0495, Japan

[b] Imaging Section, Okinawa Institute of Science and Technology (OIST) Graduate University, 1919-1 Tancha, Onna-Son, Okinawa 904-0495, Japan

[c] Department of Physics, Jai Prakash University, Chapra-841301, Bihar, India

[d] Institute of Nanosurface Science and Engineering, Shenzhen University, Nanhai Ave. 3688, Shenzhen, Guangdong, China

## Section S1: Coverage of Pd Nanoparticles (NPs)

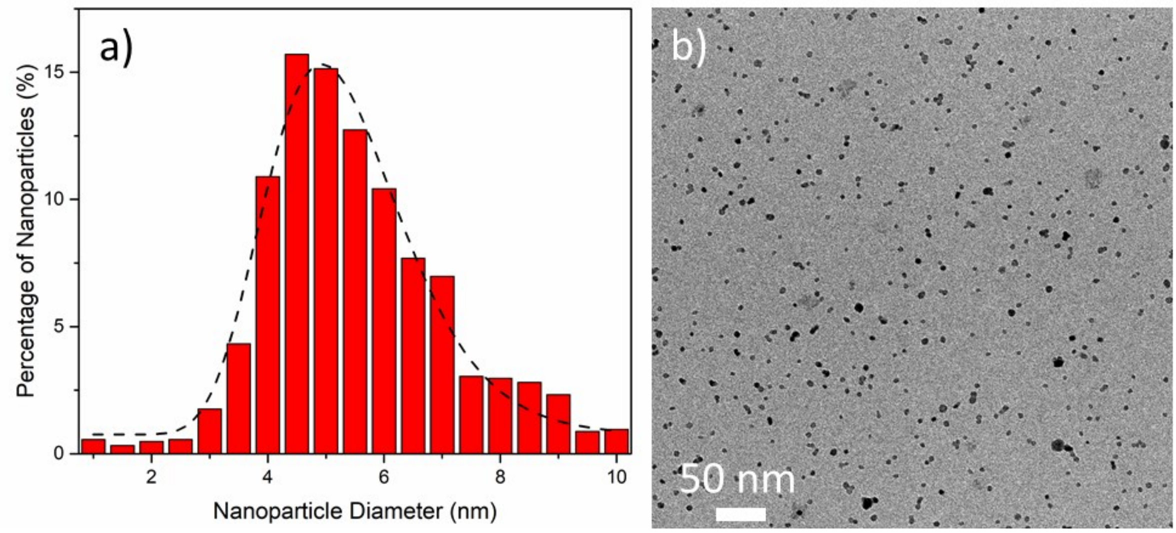

**Figure S1.** a) The size distribution of the Pd NPs deposited using magnetron assisted gas phase aggregation. b) An exemplary TEM image of Pd NPs on an amorphous carbon surface used to calculate the size and coverage achieved during deposition.

NP size was calculated using ImageJ software to determine the area of nanoparticles from multiple images like that seen in **Figure S2 b**. This was done using the same method as described by Porkovich et. Al.[1] From the area (*A*), the size as diameter (*d*) was calculated using **Equation S1**:

$$d = 2 \times \sqrt{\frac{A}{\pi}} \tag{S1}$$

These sizes were the turned into the histogram in **Figure S1 a** and fit with a log-normal curve in OriginPro 2016J.

NP coverage was calculated by multiplying the average size of each NP ($d_{av}$) by the number of nanoparticles per cm$^2$ ($\frac{n_{av}}{A_{cm^2}}$). This allows the estimation of a coverage fraction ($C_F$). **Equation S2** outlines this calculation.

$$\left(\frac{d_{av}}{2}\right)^2 \pi \times \frac{n_{av}}{A_{cm^2}} = C_F \tag{S2}$$

Averaging this over multiple images, either through the calculation of each images' coverage fraction and averaging it, or, through determining the number of NPs per cm$^2$ from each image and averaging all the values.

## Section S2: Surface Potential of Pristine and Pd-decorated CuO Nanowires (NWs)

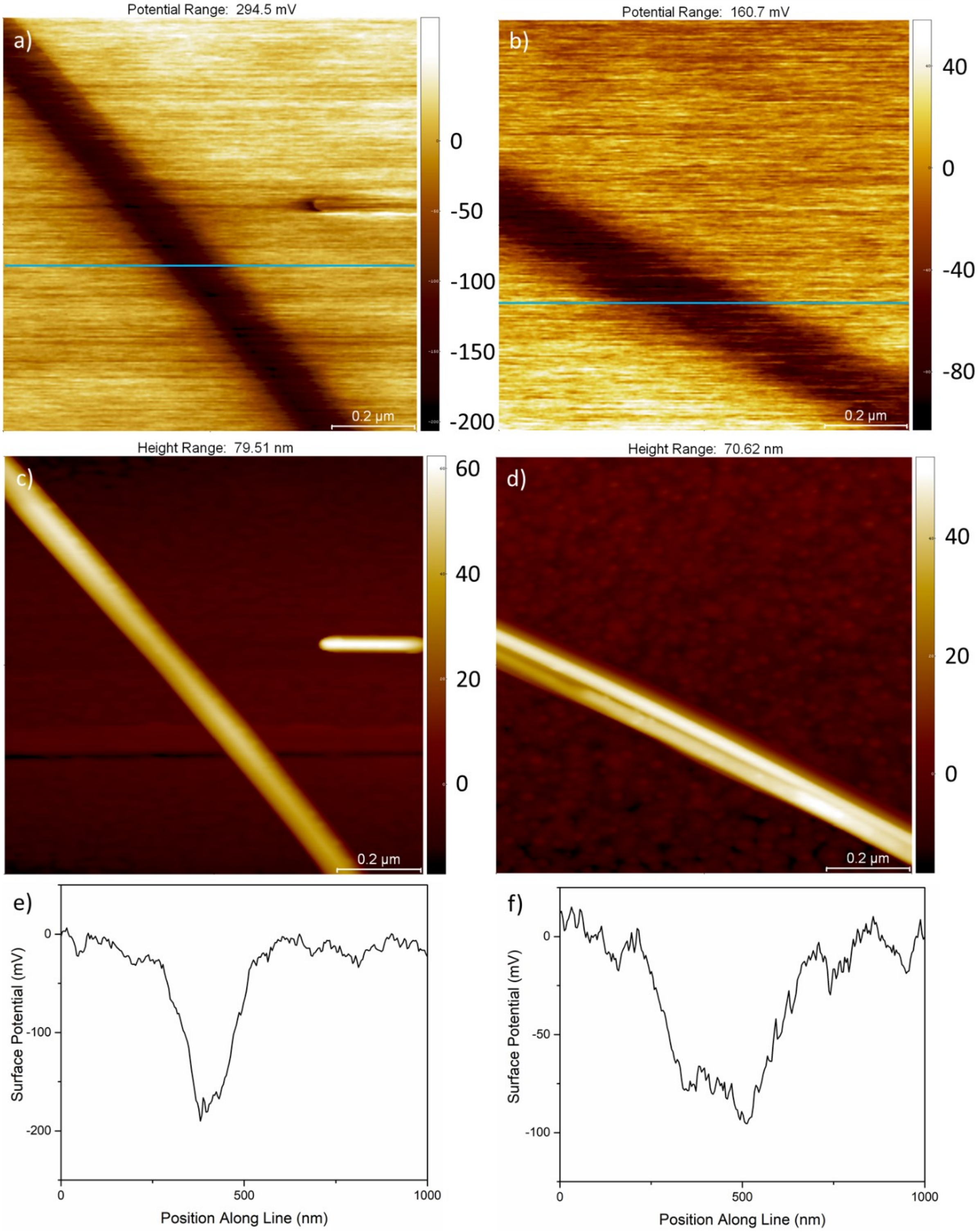

**Figure S2.** KPFM analysis of pristine and Pd-decorated CuO NWs. Surface potential (a, b) and height (c, d) images can be seen, along with line profiles (e, f) determined from the blue lines in the surface potential images. Pristine CuO NWs are seen in a), c) and e), while Pd decorated CuO NWs are displayed in b), d) and f).

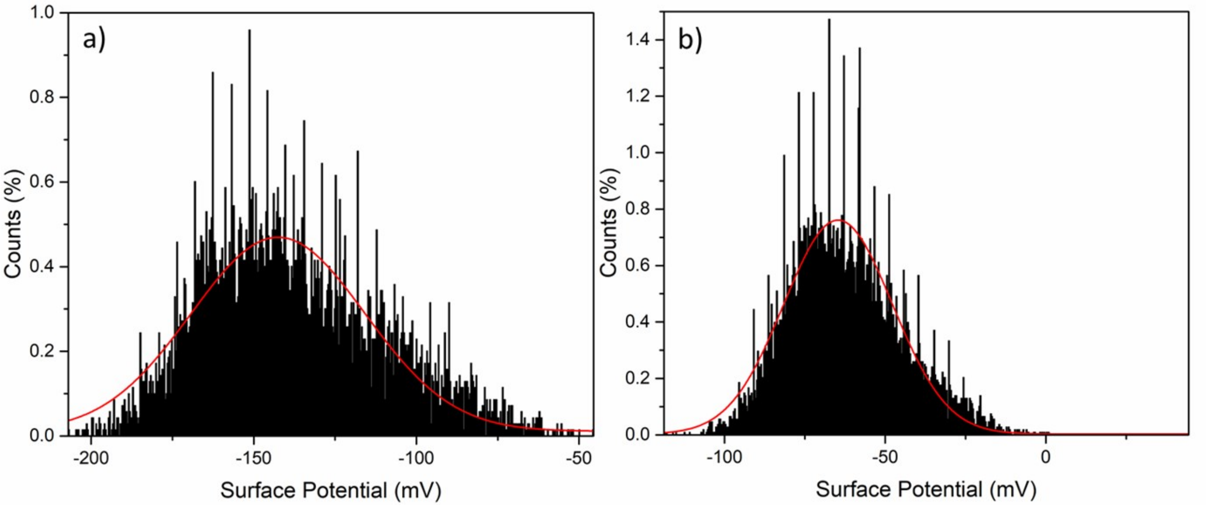

**Figure S3.** The surface potential profile shown in **Figure S2** a) and b) expressed as a histogram. Pristine (a) and Pd-decorated (b) CuO NWs can be seen with a fitted gaussian distribution to calculate the mean value which is used to estimate the surface potential of the respective CuO NWs.

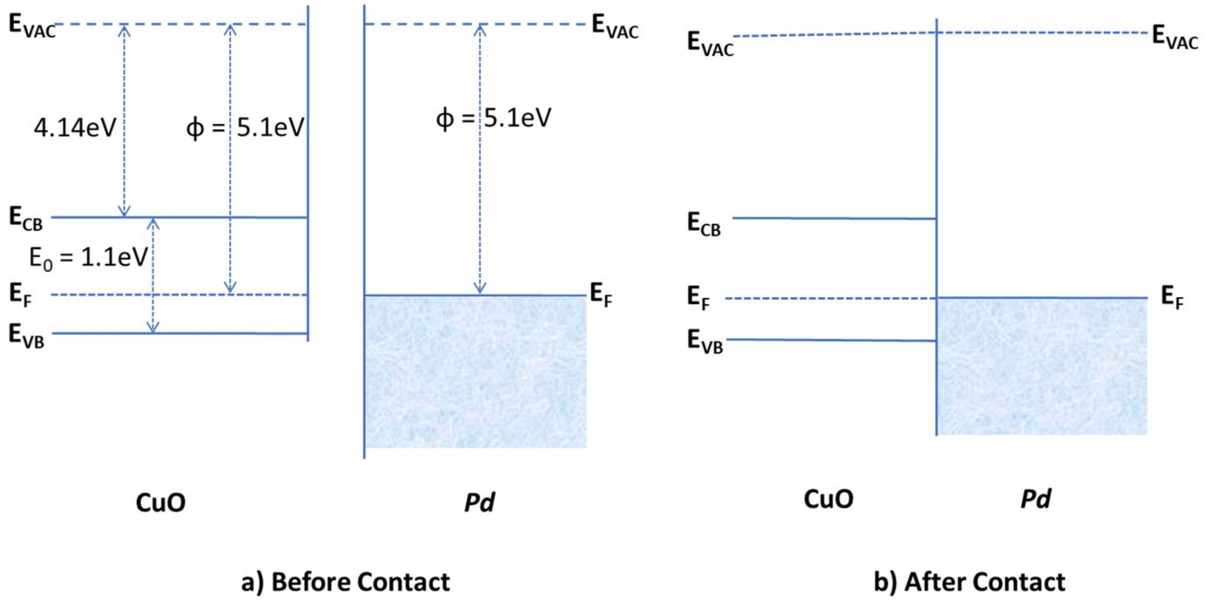

**Figure S4.** Band diagrams of CuO and Pd aligned at the vacuum level a) before contact, and at the fermi level, b) after contact. $E_{VAC}$, $E_{CB}$, $E_{VB}$ and $E_F$ represent the energy of the vacuum level, conduction band, valance band and fermi levels, respectively, while $E_0$ and φ, similarly, indicate the band gap and work function. Levels were taken from multiple literature sources for Pd[2] and CuO.[3]

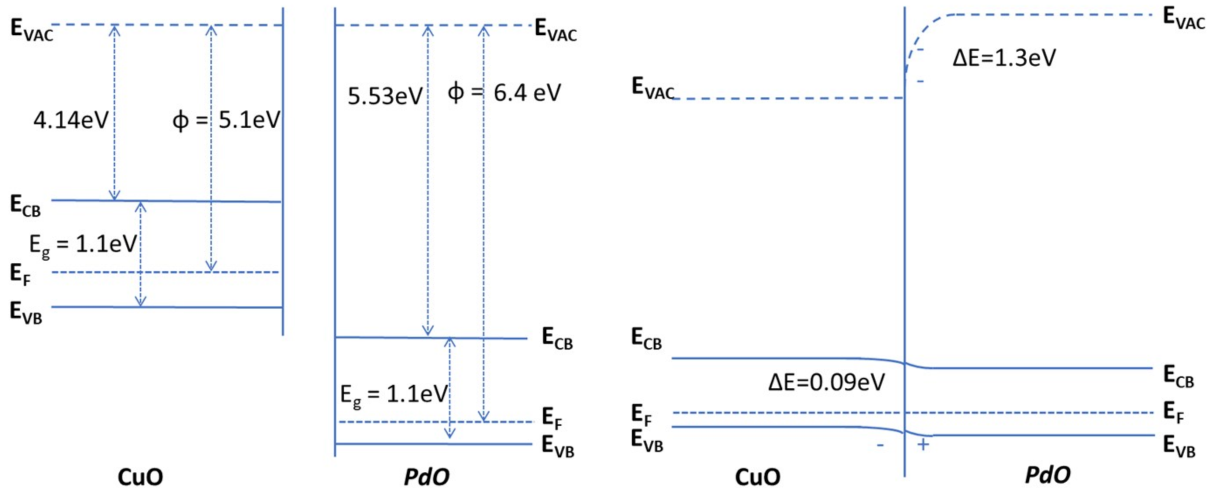

a) Before Contact

b) After Contact

**Figure S5.** Band diagrams of CuO and PdO aligned at the vacuum level a) before contact, and at the fermi level, b) after contact. $E_{VAC}$, $E_{CB}$, $E_{VB}$ and $E_F$ represent the energy of the vacuum level, conduction band, valance band and fermi levels, respectively, while $E_g$ and φ, similarly, indicate the band gap and work function. Levels were taken from multiple literature sources for CuO[3] and PdO.[4-7]

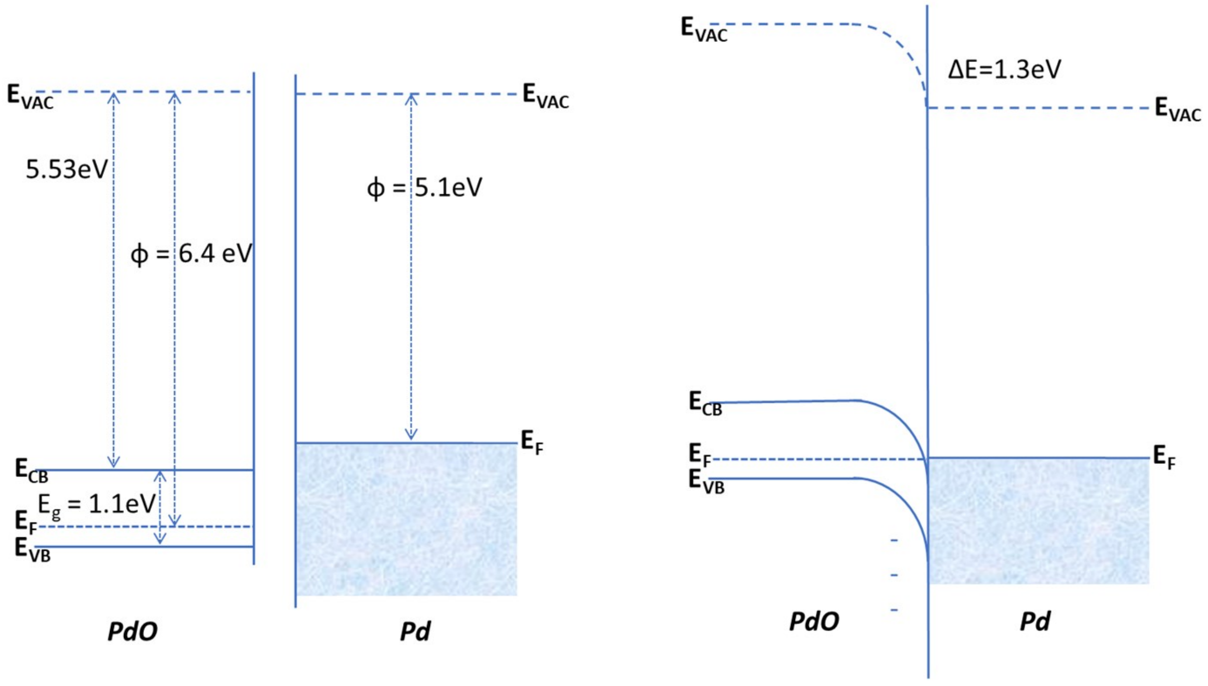

a) Before Contact

b) After Contact

**Figure S6.** Band diagrams of PdO and Pd aligned at the vacuum level a) before contact, and at the fermi level, b) after contact. $E_{VAC}$, $E_{CB}$, $E_{VB}$ and $E_F$ represent the energy of the vacuum level, conduction band, valance band and fermi levels, respectively, while $E_g$ and φ, similarly, indicate the band gap and work function. Levels were taken from multiple literature sources for PdO[4-7] and Pd.[2]

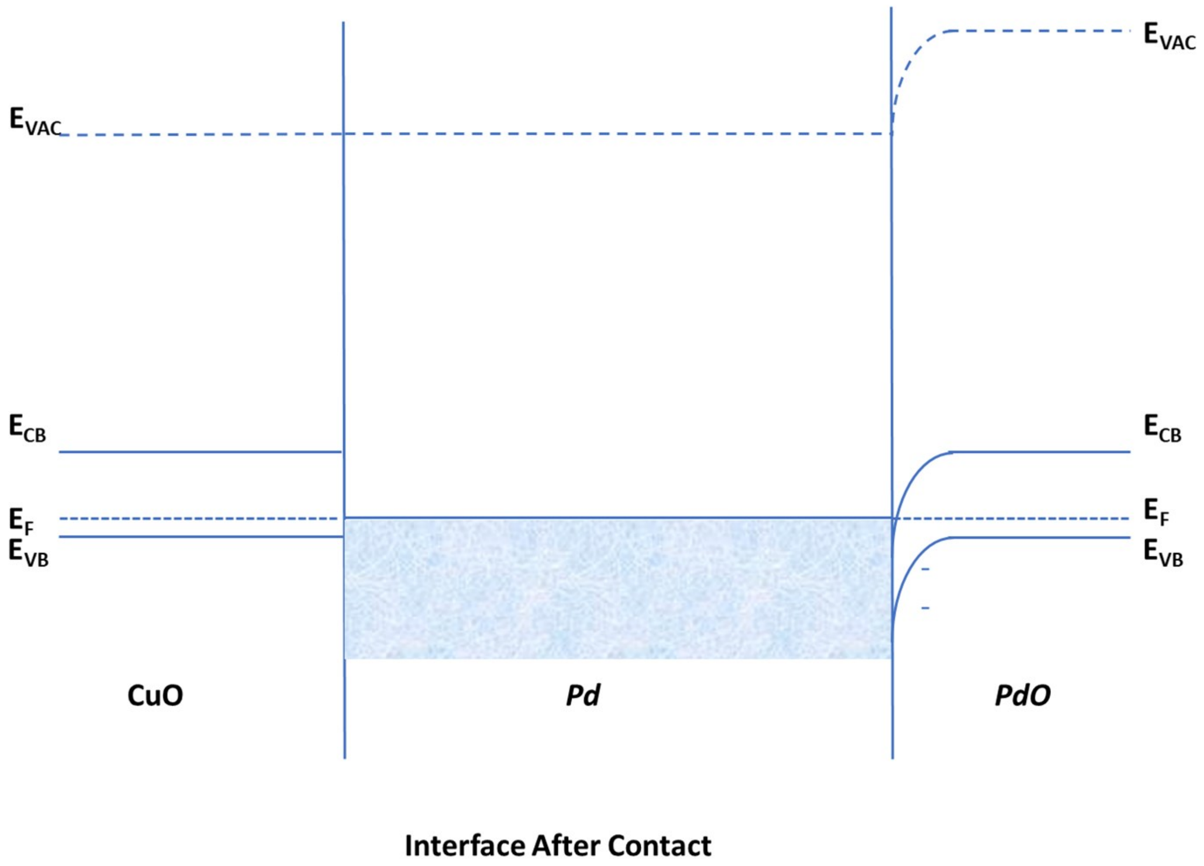

**Figure S7.** Band diagrams of CuO, Pd and PdO aligned at the fermi level after contact. $E_{VAC}$, $E_{CB}$, $E_{VB}$ and $E_F$ represent the energy of the vacuum level, conduction band, valance band and fermi levels, respectively. Levels were taken from multiple literature sources for CuO,[3] Pd[2] and PdO.[4-7]

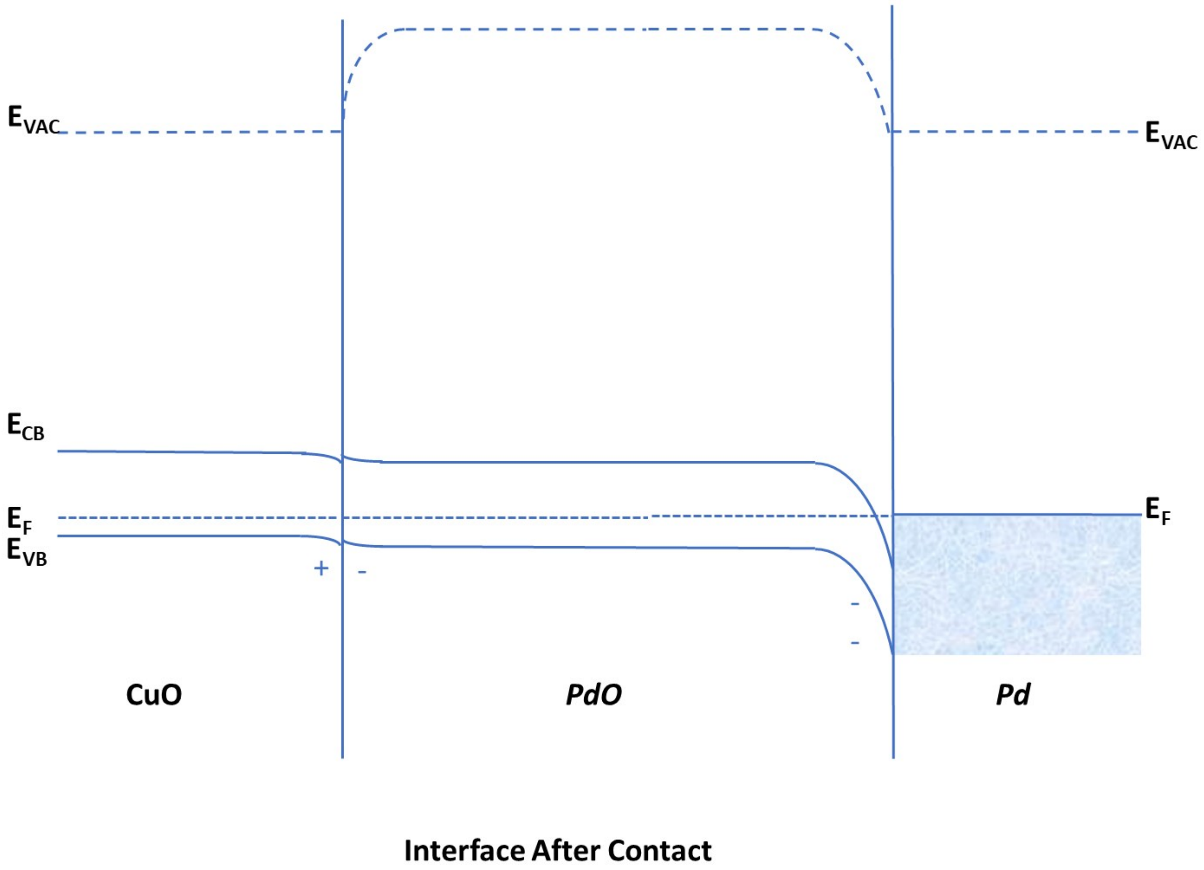

**Figure S8.** Band diagrams of CuO, PdO and Pd aligned at the fermi level after contact. $E_{VAC}$, $E_{CB}$, $E_{VB}$ and $E_F$ represent the energy of the vacuum level, conduction band, valance band and fermi levels, respectively. Levels were taken from multiple literature sources for CuO,[3] PdO[4-7] and Pd.[2]

## Section S3: *In-situ* Oxidation of Pd NPs to PdO on CuO NWs

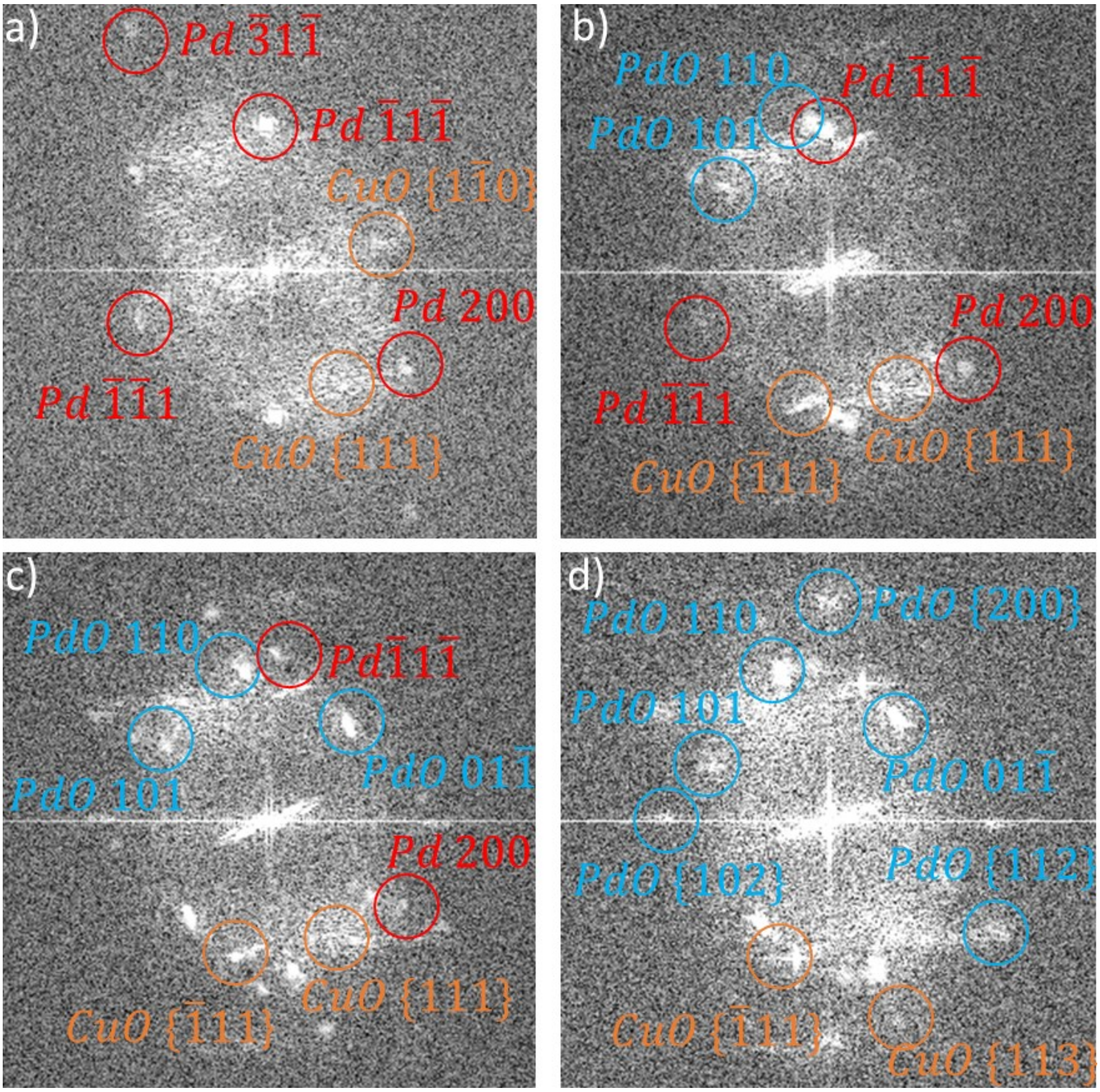

**Figure S9.** The Fast-Fourier Transforms (FFTs) of the corresponding image in figure 2 of the main text. The FFTs correspond to a beam exposure (electron dose rate of 4300 e/Å$^2$.s) times of a) 5 s, b) 110 s, c) 300 s and d) approximately 705s, along with a further 75s at a dose rate of 8000 e/Å$^2$.s. In a) and b), Pd is seen on zone axis [011], while in c) and d), PdO on zone axis is observed along the [111] direction.

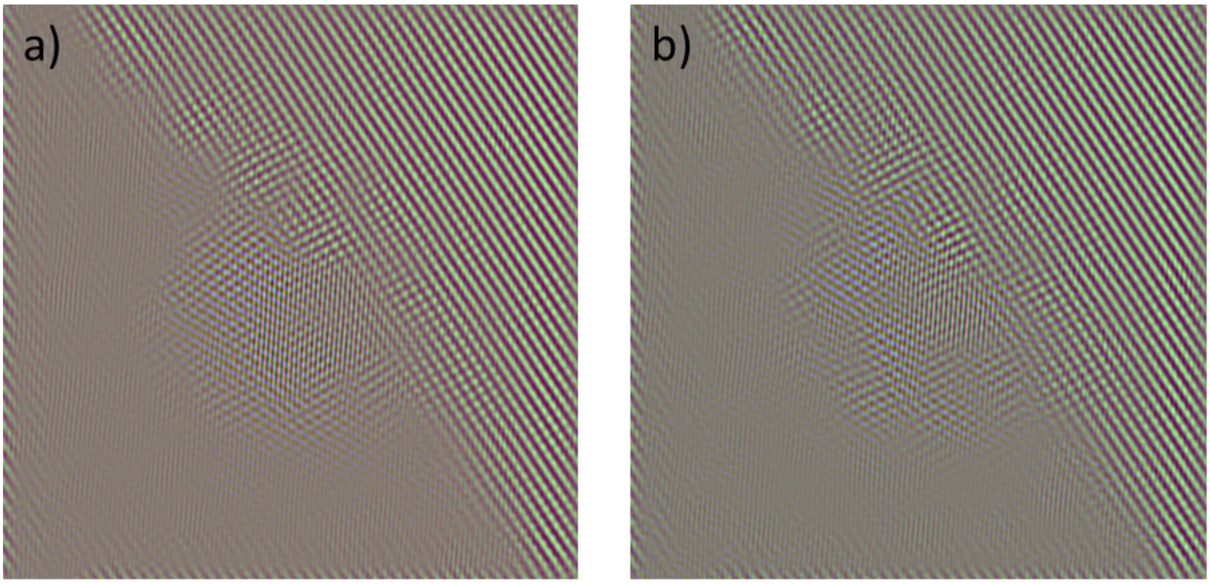

**Figure S10.** False color images created by Bragg filtering the frequencies from the corresponding FFTs related to Pd 200 (blue), Pd 311 (red) and CuO (200, 202, 002, $20\bar{2}$) (green) from figure 3 a) and b) in the main manuscript. This corresponds to an exposure time of 0 and 55s for a) and b), respectively, at an electron dose rate of 11800 e/Å$^2$.s.

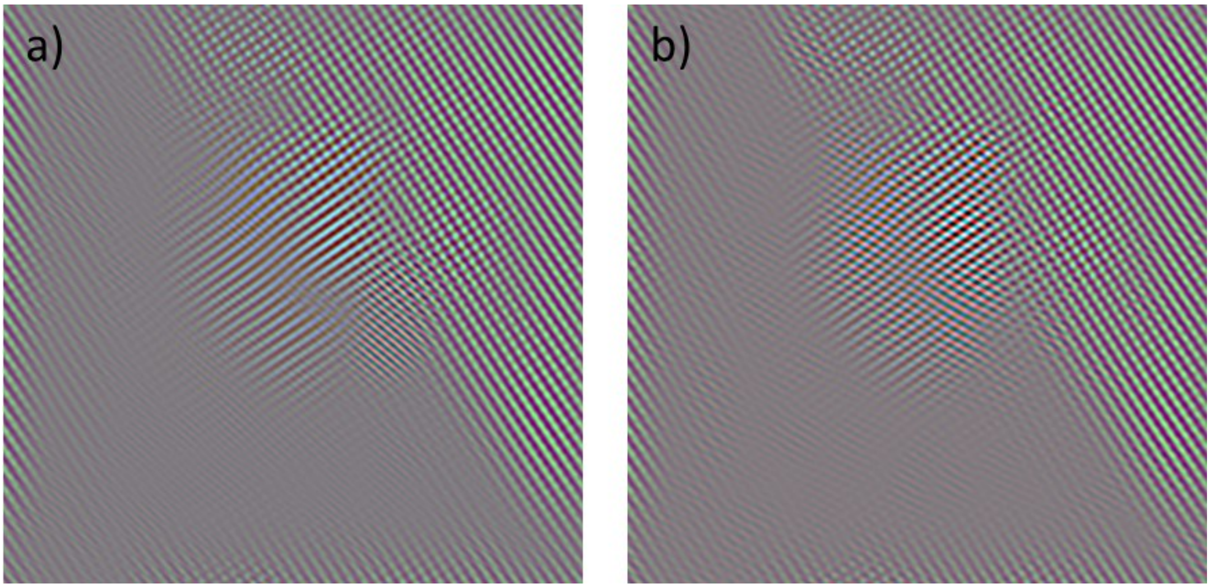

**Figure S11.** False color images created by Bragg filtering the frequencies from the corresponding FFT related to PdO 011 (blue), 200 ( red being PdO in a) and Pd in b)) and CuO (200, 202, 002, $20\bar{2}$) (green) from figure 3 c) in the main manuscript. This corresponds to an exposure time of 336s at an electron dose rate of 11800 e/Å$^2$.s.

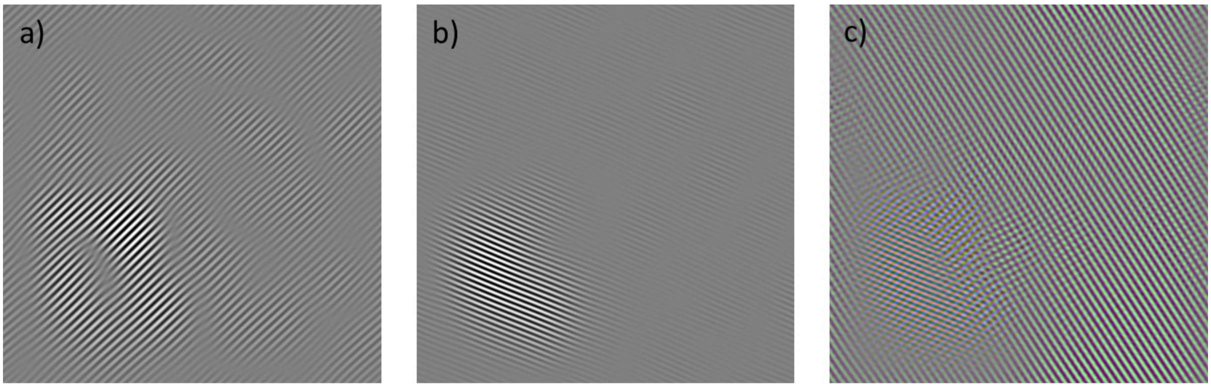

**Figure S12.** Bragg filtered and false colored images created from the frequencies in the corresponding FFT from figure 4 d) in the main manuscript. The Bragg Filtered image from frequencies corresponding to PdO 011 is seen in a), while the similar image in b) is from frequencies representing PdO $\bar{1}11$. The false colored image in c) is created from frequencies relating to PdO 011 (blue), PdO $\bar{1}11$ (red) and CuO (200, 202, 002, $20\bar{2}$) (green). This image corresponds to an exposure time of 1341s, at an electron dose rate of 11800 e/Å$^2$.s.

## Section S4: *In situ* X-ray Photoelectron Spectroscopy (XPS)

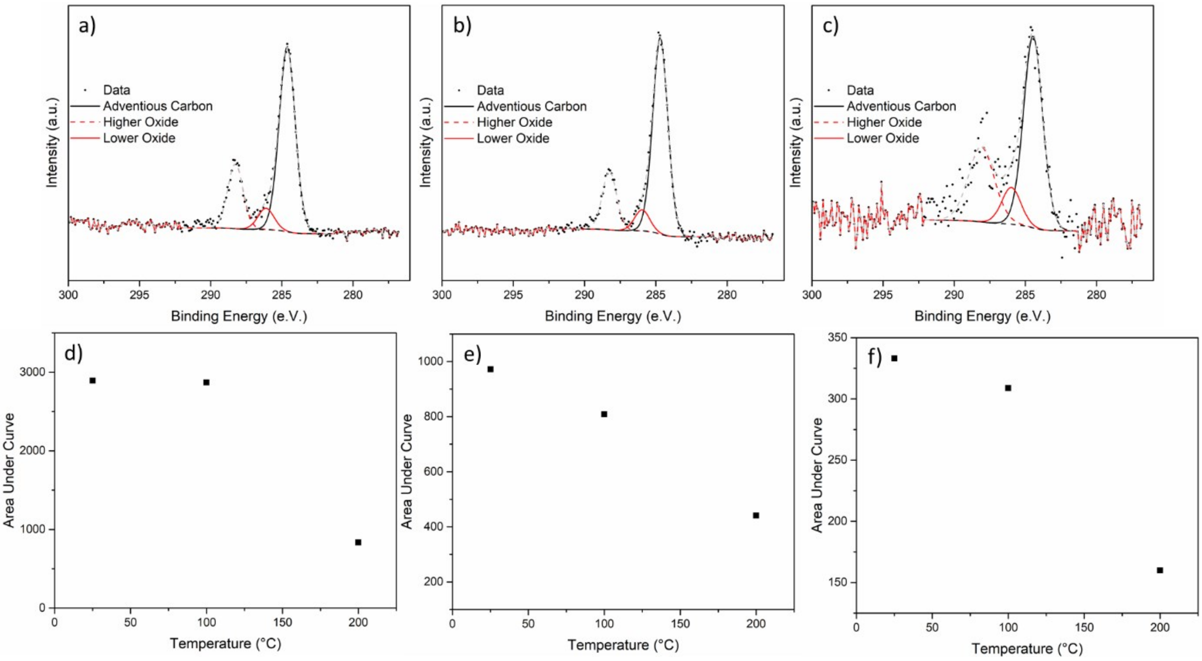

**Figure S13.** The changes in the carbon 1s XPS peak during heating in vacuum, as seen from samples a) as-deposited, b) annealed at 100°C and c) annealed at 200°C. The concentration of each carbon species is determined by the area under the curve of the deconvolution. The changing concentration of each species at each temperature can be seen for d) adventitious carbon, e) the higher energy oxide, and f) the lower energy oxide.

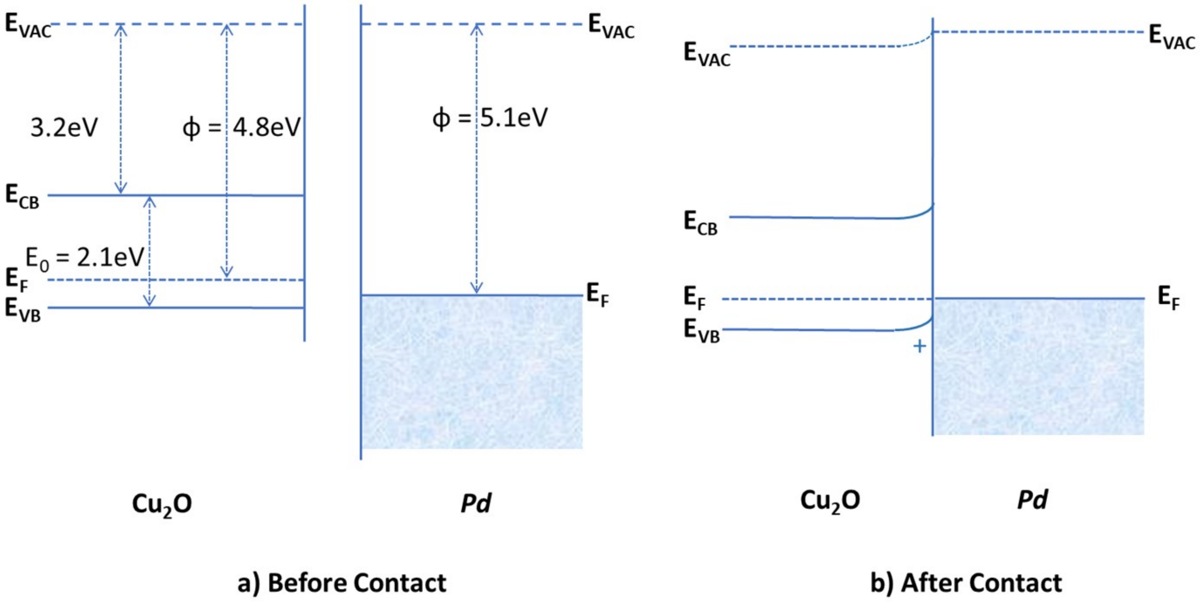

**a) Before Contact**

**b) After Contact**

**Figure S14.** Band diagrams of $Cu_2O$ and Pd aligned at the vacuum level a) before contact, and at the fermi level, b) after contact. $E_{VAC}$, $E_{CB}$, $E_{VB}$ and $E_F$ represent the energy of the vacuum level, conduction band, valance band and fermi levels, respectively, while $E_0$ and φ, similarly, indicate the band gap and work function. Levels were taken from multiple literature sources for $Cu_2O$[3, 10-12] and Pd.[2]

## Section S5: Scanning Transmission Electron Microscopy (STEM) of post vacuum heated Pd NPs on CuO NWs

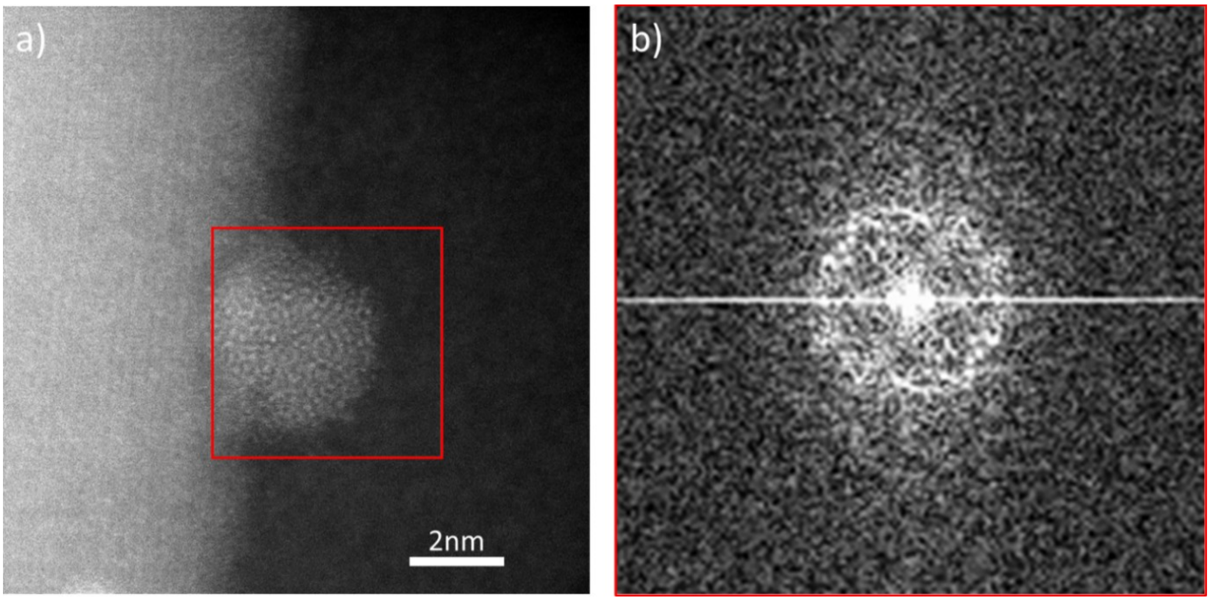

**Figure S15.** a) An example of a Pd NP post vacuum heating treatment can be seen in the red square. This particle is clearly amorphous, as confirmed by b) the FFT of the selected area within the red square. The lack of any specific special frequencies indicates that there is no crystal ordering, hence, the Pd is amorphous.

## Section S6: STEM and XPS Characterization of Pd NPs on Si supports.

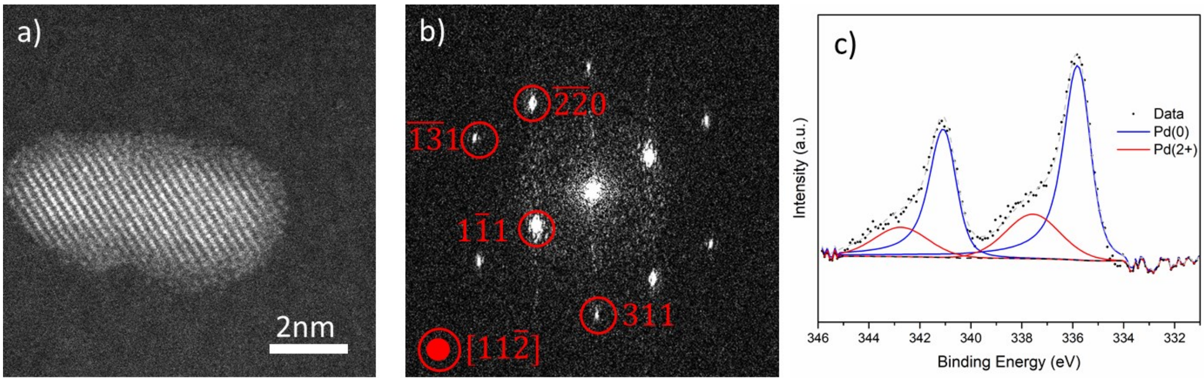

**Figure S16.** An example of Pd NPs as deposited on SiN TEM grids can be seen in a). The NPs are found to have a crystalline face-centered cubic (fcc) lattice structures, like that of the bulk literature values of Pd, when viewed on the $[11\bar{2}]$ zone axis. This was determined from the FFT of the local area of the NP as seen in b). Finally, Pd NPs as deposited on Si Substrates were examined using XPS, with the Pd 3d peak displayed in c). The C 1s peak is calibrated to 248.8 eV, and the metallic (Pd(0)) and oxide (Pd(2+)) components were found at 335.6 eV[8] and 337.2 eV[9] respectively, with a standard spin orbit split of 5.3 eV, as is characteristic of Pd.[8] Shirley background is represented using a dotted black line, while the sum of the deconvolution peaks is represented as the dotted grey line. The metallic component is fitted with an asymmetric line shape LF(0.8, 1.25, 500, 180), while the oxide component is a symmetrical GL(30) fit.[8, 9]

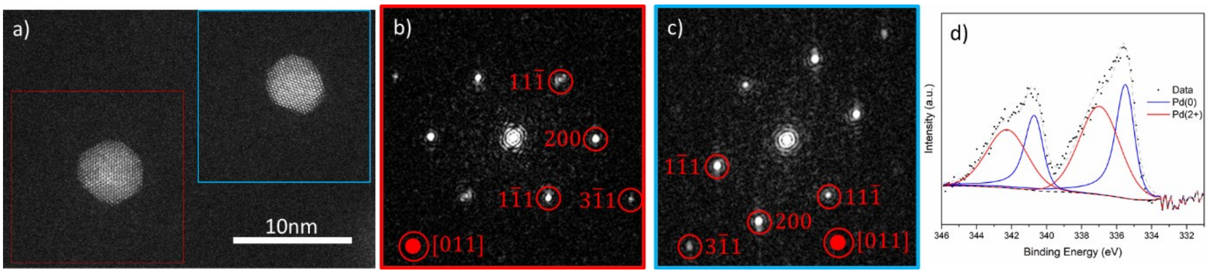

**Figure S17.** An example of Pd NPs following a 200°C annealing in an ambient environment for 30 minutes on SiN TEM grids can be seen in a). The NPs are found to have a crystalline face-centered cubic (fcc) lattice structures, like that of the bulk literature values of Pd, when viewed on the $[011]$ zone axis. This was determined from the FFT of the local area of the NPs and surrounding as seen in b) and c). Each The color of the box surrounding each NP indicates which FFT belongs to which. Finally, Pd NPs Si Substrates were annealed at 200°C in an ambient environment, and examined using XPS, with the Pd 3d peak displayed in d). The C 1s peak is calibrated to 248.8 eV, and the metallic (Pd(0)) and oxide (Pd(2+)) components were found at 335.6 eV[8] and 337.2 eV[9] respectively, with a standard spin orbit split of 5.3 eV, as is characteristic of Pd.[8] Shirley background is represented using a dotted black line, while the sum of the deconvolution peaks is represented as the dotted grey line. The metallic component is fitted with an asymmetric line shape LF(0.8, 1.25, 500, 180), while the oxide component is a symmetrical GL(30) fit.[8, 9]

## Section S7: Supplementary Information References

1. Porkovich, A.; Ziadi, Z.; Kumar, P.; Kioseoglou, J.; Jian, N.; Weng, L.; Steinhauer, S.; Vernieres, J.; Grammatikopoulos, P.; Sowwan, M., In Situ Observation of Metal to Metal Oxide Progression: A Study of Charge Transfer Phenomenon at Ru-CuO Interfaces. *ACS Nano* 2019, *13*, 12425-12437.
2. Tani, T., Analysis of Work Functions of Noble Metals in Ambient Atmosphere in Commemoration of Journal Award. *J. Soc. Photogr. Imag. Japan.* 2015, *78*, 16-22.
3. Heinemann, M.; Eifert, B.; Heiliger, C., Band structure and phase stability of the copper oxides Cu2O, CuO, and Cu4O3. *Physical Review B* 2013, *87*.
4. Acharyya, D.; Huang, K. Y.; Chattopadhyay, P. P.; Ho, M. S.; Fecht, H. J.; Bhattacharyya, P., Hybrid 3D structures of ZnO nanoflowers and PdO nanoparticles as a highly selective methanol sensor. *Analyst* 2016, *141*, 2977-89.
5. Majhi, S. M.; Lee, H.-J.; Choi, H.-N.; Cho, H.-Y.; Kim, J.-S.; Lee, C.-R.; Yu, Y.-T., Construction of novel hybrid PdO–ZnO p–n heterojunction nanostructures as a high-response sensor for acetaldehyde gas. *CrystEngComm* 2019, *21*, 5084-5094.
6. Rogal, J.; Reuter, K.; Scheffler, M., Thermodynamic stability of PdO surfaces. *Physical Review B* 2004, *69*.
7. Wang, L.; Lou, Z.; Wang, R.; Fei, T.; Zhang, T., Ring-like PdO–NiO with lamellar structure for gas sensor application. *Journal of Materials Chemistry* 2012, *22*, 12453.
8. Militello, M. C.; Simko, S. J., Elemental Palladium by XPS. *Surface Science Spectra* 1994, *3*, 387-394.
9. Militello, M. C.; Simko, S. J., Palladium Oxide (PdO) by XPS. *Surface Science Spectra* 1994, *3*, 395-401.